Numerical study of the spin up of a tropical low over land during the Australian monsoon

Shengming Tang[a], Roger K. Smith[b] *, Michael T. Montgomery[c] and Ming Gu[a]
[a] *State Key Laboratory for Disaster Reduction in Civil Engineering, Tongji University, Shanghai, China*
[b] *Meteorological Institute, Ludwig-Maximilians University of Munich, Munich, Germany*
[c] *Dept. of Meteorology, Naval Postgraduate School, Monterey, CA.*
*Correspondence to: Prof. Roger K. Smith, Meteorological Institute, Ludwig-Maximilians University of Munich, Munich, Germany. E-mail: roger.smith@lmu.de

An analysis of numerical simulations of tropical low intensification over land is presented. The simulations are carried out using the MM5 mesoscale model with initial and boundary conditions provided by ECMWF analyses. Seven simulations are discussed: a control simulation, five sensitivity simulations in which the initial moisture availability is varied, and one simulation in which the coupling between moisture availability is suppressed. Changing the initial moisture availability adds a stochastic element to the development of deep convection. The results are interpreted in terms of the classical axisymmetric paradigm for tropical cyclone intensification with recent modifications.
Spin up over land is favoured by the development of deep convection near the centre of the low circulation. As for tropical cyclones over sea, this convection leads to an overturning circulation that draws absolute angular momentum surfaces inwards in the lower troposphere leading to spin up of the tangential winds above the boundary layer. The intensification takes place within a moist monsoonal environment, which appears to be sufficient to support sporadic deep convection. A moisture budget for two mesoscale columns of air encompassing the storm shows that the horizontal import of moisture is roughly equal to the moisture lost by precipitation. Overall, surface moisture fluxes make a small quantitative contribution to the budget, although near the circulation centre, these fluxes appear to play an important role in generating local conditional instability. Suppressing the effect of rainfall on the moisture availability has little effect on the evolution of the low, presumably because, at any one time, deep convection is not sufficiently widespread.

Key Words: Tropical low, landphoon, agukabam, spin-up, intensification, spin up mechanisms

Received February 22, 2016

Citation: . . .

1. Introduction

Early in the Australian wet season, the monsoon trough generally lies over the seas to the north of the Australian continent, but as the season advances, it often moves south over the continent. It is typical for low pressure systems to develop at spatial intervals along the trough and since water temperatures to the north of Australia can be up to 30^{o}C, some of the lows that develop over the ocean develop into tropical cyclones. Lows that form over land are sometimes referred to as monsoon lows or monsoon depressions.

In general, tropical cyclones normally weaken after landfall as the supply of latent heat from the ocean surface is cut off and the surface friction increases. However,

there have been recorded cases of storms re-intensifying over land after initially weakening (Emanuel et al. 2008; Arndt et al. 2009; Brennan et al. 2009; Evans et al. 2011). Moreover, some tropical cyclones around the northern coast of Australia originate from tropical lows that first form over land before moving over the sea and intensifying further (e.g. Tory et al. 2007; Smith et al. 2015a). Even if they remain over land, tropical lows often give rise to prodigious amounts of rainfall and can cause serious flooding over a wide area. Since comparatively little has been known in detail about their formation pathways and structure, these lows pose significant challenges to forecasters. One question is to what extent the formation, structure and intensification of these lows over land are similar to those of tropical cyclones over sea?

An early pioneering and insightful analysis of tropical cyclogenesis in the Australian region is provided by McBride and Keenan (1982) and since then there have been one or two early case studies of lows that initially formed over land (Foster and Lyons 1984; Davidson and Holland 1987).

Emanuel et al. (2008) pointed out that even in the absence of appreciable extratropical interactions, and although the underlying soil is desert sand, some cyclones making landfall over northern Australia may re-intensify to the point of reacquiring the classical inner-core structure of a cyclone, including an eye. They presented a case study of such an event (Tropical Cyclone Abigail 2001). They hypothesized that the intensification or re-intensification of these systems, which they christened "agukabams", is made possible by large vertical heat fluxes from a deep layer of very hot, sandy soil that has been wetted by the first rains of the approaching systems, significantly increasing its thermal diffusivity. In support of this hypothesis, they presented results simulations with a simple axisymmetric tropical cyclone model coupled to a one-dimensional soil model. These axisymmetric simulations indicated that warm-core cyclones could intensify when the underlying soil is sufficiently warm and wet and are maintained by latent heat transfer from the soil. The simulations suggested also that when the storms are sufficiently isolated from their oceanic source of moisture, the rainfall they produce is insufficient to keep the soil wet enough to transfer significant quantities of latent heat, and the storms then decay rapidly.

Evans et al. (2011) carried out numerical simulations of Tropical Storm Erin (2007), which made landfall as a tropical depression from the Gulf of Mexico and underwent re-intensification as it moved northeastwards over the central United States (Arndt et al. (2009), Brennan et al. (2009)). They found that the Emanuel et al. (2008) along-track tropical cyclone rainfall feedback mechanism to be of minimal importance to the evolution of the vortex. They concluded that " ... the final intensity of the simulated (and presumably observed) vortex appears to be closely linked to the maintenance of boundary layer moisture over preexisting near-climatological soil moisture content along the track of the vortex and well above climatological soil moisture content". Citing Montgomery et al. (2009) they noted that tropical cyclone development over water requires only a modest elevation of surface latent heat fluxes beyond those of nominal trade-wind values on the order of 150 W m^{-2}: it does not require these fluxes to continue to increase with increasing wind speed (see also Montgomery et al. 2015), which would appear to be an essential feature of the axisymmetric model used by Emanuel et al. (2008).

Interestingly, Evans et al. (2011) did speculate that "... the development and organization of deep moist convection near the center of the vortex is necessary - and perhaps sufficient - for vortex re-intensification to occur". While they did not show details of the convection, they did show an increase in "the temporally and area-integrated vertical mass flux" within a column 100×100 km^2 centered on the simulated vortex in all their simulations (their Fig. 18).

During the last decade, advances in understanding maritime tropical cyclogenesis have emerged from seminal studies by Hendricks et al. (2004), Montgomery et al. (2006), and Dunkerton et al. (2009). A review of this and other research on the topic was given by Montgomery and Smith (2011). Hendricks et al. (2004) and Montgomery et al. (2006) drew attention to the important role of rotating deep convection during genesis, while Dunkerton et al. (2009) examined the nurturing role of a tropical wave and presented a new framework for understanding how such hybrid wave-vortex structures develop into tropical depressions. Rotating deep convection has been shown to be a feature also of the subsequent intensification of tropical cyclones (Nguyen et al. 2008; Montgomery et al. 2009; Smith et al. 2009; Bui et al. 2009; Fang and Zhang 2010; Persing et al. 2013). In this paper we examine an alternative hypothesis to Emanuel et al. (2008): namely that the formation and intensification or re-intensification of tropical lows over land in a monsoonal environment is a similar process to that which occurs over the sea and is not dependent on special properties of the soil.

A relatively well observed example of a low that developed near the coast and intensified as it drifted inland is the one that formed near the north coast of Australia during the Tropical Warm Pool International Cloud Experiment (TWP-ICE) in January 2006 (May et al. 2008). This low passed over Darwin, the focal point for the experiment, before moving inland and intensifying as it moved southwards over several days. In its early stages, the low was well sampled by a network of radiosonde soundings in the Darwin region, data which should have benefited global analyses of the low at these stages. However, the subsequent intensification took place over a relatively data sparse region of the Northern Territory where reliance on analyses of the global models for storm behaviour is required. In this paper we present a series of numerical simulations of this low, which captured the inland intensification as seen in the European Centre for Medium Range Weather Forecasts analyses (ECMWF) for the event. Analyses of these simulations indicate that, indeed, the intensification does conform with the new paradigm for the intensification of maritime storms summarized recently by Montgomery and Smith (2014) and Smith and Montgomery (2015b).

The remainder of the paper is structured as follows. Section 2 gives an overview of the tropical low and section 3 gives a brief description of the numerical model. Section 4 describes the vortex development in the numerical simulations. Section 5 examines the basic dynamics of vortex spin up in an axissymmetric framework. Section 6 examines the reasons for the differences in behaviour for all sensitivity simulations on the second day and section 7 investigates aspects of the thermodynamic support for spin up. The conclusions are given in section 8.

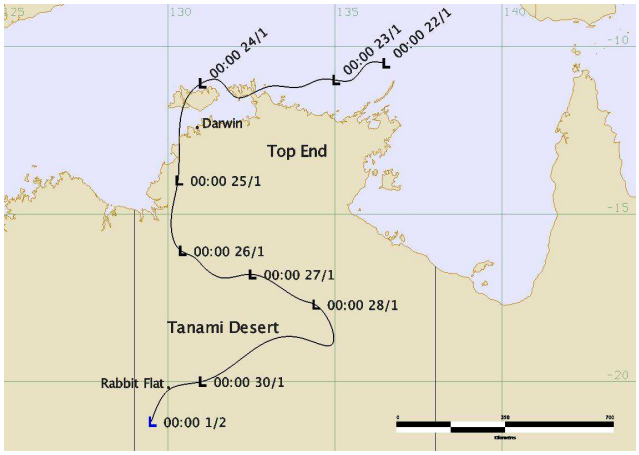

Figure 1. Best-track position of NT2006 with place names mentioned in the text. (Image courtesy of Ian Shepherd, Northern Territory Regional Office, Australian Bureau of Meteorology)

2. Overview of the tropical low

The case chosen for investigation herein is an unnamed low (subsequently referred to as "NT2006") that formed off the north coast of the Northern Territory around 00:00 UTC* 22 Jan during the TWP-ICE. During the following two days it moved westwards and strengthened into a tropical storm, making landfall in the Darwin area around 18:00 UTC 24 Jan, before drifting down the western border of the Northern Territory. After landfall, the low moved southwards and weakened, but around 00:00 UTC 26 Jan, it began to track southeastwards and re-intensified, achieving its maximum strength at 00:00 UTC 28 Jan. Thereafter it gradually weakened over land and from 00:00 UTC 29 Jan it began to move slowly southwestwards. The low initiated an active monsoon onset over the Top End and brought heavy rainfall to many parts of the western Northern Territory, including some areas of the Tanami Desert, which exceeded their annual average rainfall in a few days. There was heavy rainfall in the Darwin region also, with many 24 hour totals exceeding 100 mm. Figure 1 shows the best-track position of NT2006 from 00:00 UTC 22 Jan to 00:00 UTC 1 February. The only observational data on the intensity of the low came from the Bureau of Meteorology's automatic weather station at Rabbit Flat, where near surface sustained winds of 15 m s^{-1} and 16 m s^{-1} were recorded at 08:00 UTC and 11:00 UTC on 31 Jan, respectively.

Figure 2 shows the time series of the minimum sea-level pressure, P_{min}, and maximum total (horizontal) wind speed at 850 mb, V_{max}, of NT2006, obtained from the ECMWF analyses. Based on these time series, we can identify three stages of evolution: (1) the first stage is from 18:00 UTC 24 Jan to 00:00 UTC 26 Jan during which time the vortex intensity at 850 mb has a time mean value of about 19 m s^{-1} and the time mean value of P_{min} is about 999 mb; (2) the second stage is from 00:00 UTC 26 Jan to 00:00 UTC 28 Jan during which P_{min} begins to fall steadily and V_{max} increases to about 31 m s^{-1}; (3) the third stage is from 00:00 UTC 28 Jan to 06:00 UTC 29 Jan during which P_{min} steadily increases and V_{max} steadily decreases. It is during the second stage that NT2006 re-intensified over land. This period will be the focus of the present paper.

*Universal Time Coordinated.

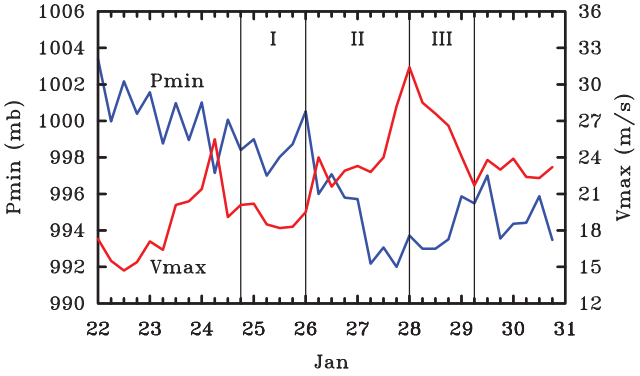

Figure 2. Time series of the minimum sea-level pressure, P_{min}, and maximum horizontal total wind speed at the height of 850 mb, V_{max}, of NT2006 as seen in the ECWMF analyses.

3. The model configuration

The numerical experiments are performed using the Pennsylvania State University/National Center for Atmospheric Research fifth-generation Mesoscale Model (MM5 version 3.6.1). MM5 is a non-hydrostatic sigma-coordinate model designed to simulate or predict mesoscale atmospheric circulations (Dudhia 1993; Grell et al. 1995). The model is configured here with two domains: a one-way nested outer domain of 9 km grid spacing, and a two-way nested inner domain of 3 km grid spacing with the centre located at 16°S,132.5°E. The domains are rectangular and have 201×203 and 493×505 grid points for the outer domain and inner domain, respectively. There are 23 σ-levels in the vertical direction†. Ten of these levels cover the region from the surface to 850 mb to provide an adequate vertical resolution for representing the planetary boundary layer. The pressure of the model top, p_{top}, is set to 100 mb.

The planetary boundary-layer is modelled using the Hong-Pan scheme (Hong and Pan 1996) and deep moist convection is represented explicitly using a simple-ice scheme (Dudhia 1993). No cumulus parameterization is used. The cloud-radiation scheme is used as a radiative cooling scheme and the five-layer soil model is used as a surface scheme.

In MM5, the surface evaporation depends on a parameter called moisture availability (M_a)‡ which is used to represent the effects of stomatal resistance, aerodynamic resistance and soil moisture (Eckel 2002). In the control experiment, the initial value of M_a in a certain model grid box is obtained from a look-up table based on the land type and season (Dudhia et al. 2005, Table 4.2c). The main land types for the present MM5 simulation are savanna, water bodies and shrub land (Figure 3), whose default M_a values are 15%, 10% and 100% in the northern summer.

The initial data and boundary conditions are provided by the ECMWF analyses.

†The values of σ are: 0.9975, 0.9925, 0.985, 0.975, 0.965, 0.955, 0.94, 0.92, 0.9, 0.87, 0.83, 0.79, 0.75, 0.71, 0.67, 0.63, 0.59, 0.55, 0.51, 0.47, 0.375, 0.225 and 0.075

‡Specifically, the formula for the moisture availability is $M_a = E/[C_E V_1 \rho(q_0^* - q_1)]$, where E is the surface evaporation rate [unit kg m^{-2} s^{-1}], C_E is the moisture exchange coefficient, V_1 is the wind speed [unit m s^{-1}] at a height h_1 [unit m] at which the wind speed and moisture are measured, ρ is the air surface density [unit kg m^{-3}], q_0^* is the saturation mixing ratio at the surface and q_1 is the mixing ratio at height h_1, typically 2 m, the lowest model level (Eckel 2002).

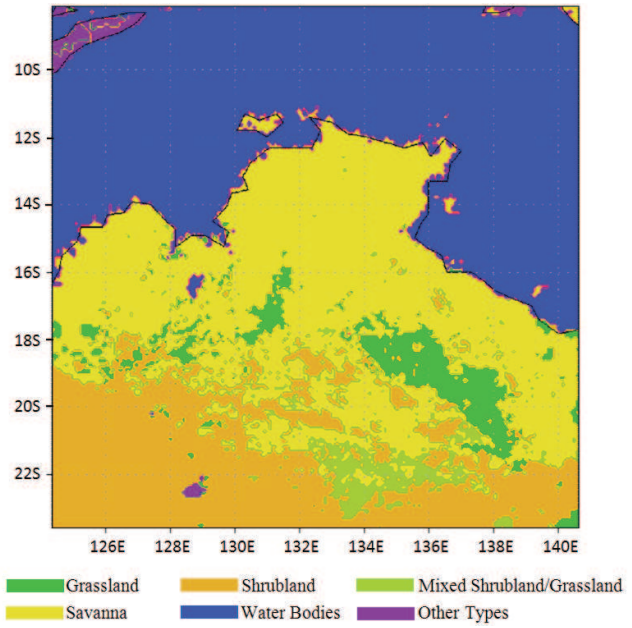

Figure 3. MM5 land use for the outer domain

3.1. *Sensitivity experiments*

As suggested by previous studies, it is reasonable to expect that the surface evaporation rate would be an important element in the intensification of tropical lows over land since, in order to maintain deep convection, there has to be a mechanism to replenish the moisture that convection consumes. However, over land, the surface evaporation depends on the surface moisture, a quantity that is not routinely measured. For this reason, in the calculations to be described, we examine the sensitivity of the calculations to the initial moisture availability. Altogether, seven calculations are presented: a control experiment and six other experiments, which are detailed in Table I. In all experiments except C6, the bucket soil moisture scheme[§] is used so that M_a is allowed to vary with space and time in response to rainfall and evaporation rates. In experiment C6, M_a is held fixed: it is not allowed to vary with time in response to rainfall and evaporation rate.

The MM5 integrations all commence at 00:00 UTC 26 Jan and run for 48 h. Data are examined at time intervals of 5 min. The results are presented in the next section.

4. The numerical simulations

4.1. *Overview of vortex development*

We present first an overview of the storm's intensification after landfall (stage II) in the control simulation and in the additional sensitivity simulations. Figure 4a shows time series of the minimum sea-level pressure P_{min} for both ECMWF analyses and MM5 simulations C0-C6. Figures 4b and 4c show the maximum total wind speed VT_{max} and maximum azimuthally-averaged tangential wind component V_{max} at 900 mb (approximately 870 m high) respectively. The azimuthal average is calculated relative to the vortex centre, defined here as the location of the minimum sea-level pressure[¶] within a radius of 150 km.

The MM5 calculations begins at 00:00 UTC 26 Jan, 30 hours after the storm made landfall. On 25 Jan, the storm intensity in the ECMWF analysis was quasi-steady with P_{min} increasing slightly from 999 mb to 1000.6 mb, VT_{max} lying around 19 m s^{-1} and V_{max} around 9 m s^{-1}.

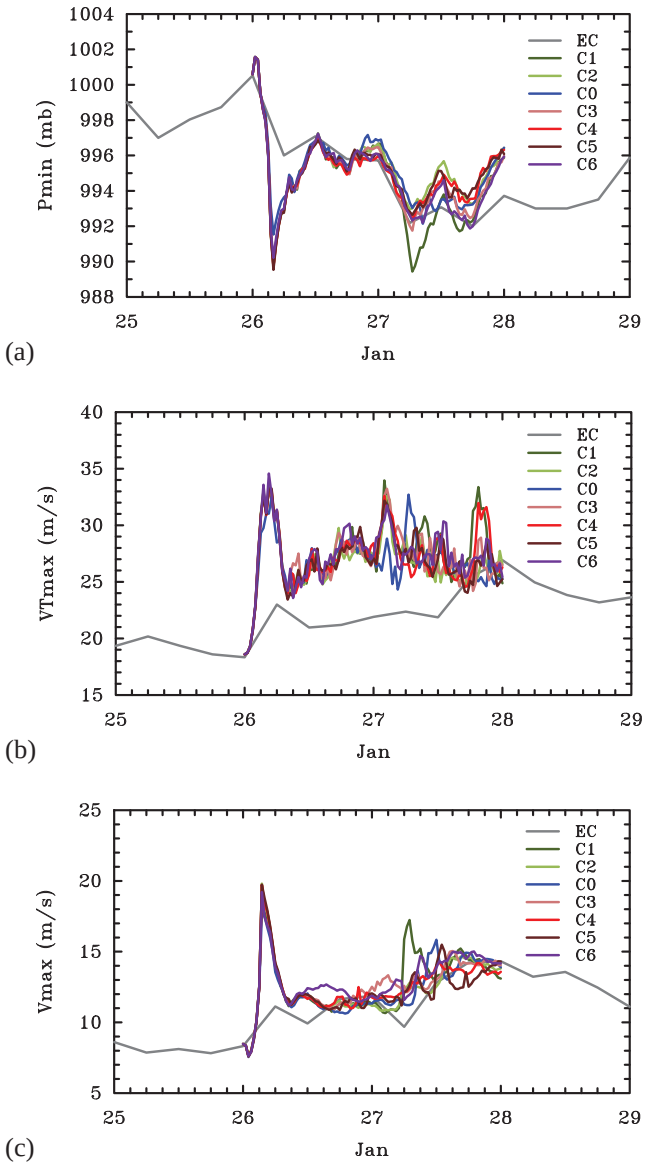

Figure 4. Vortex development in both ECMWF analyses and MM5 simulations C0-C6. Time series of: (a) minimum sea-level pressure P_{min}; (b) maximum total wind speed VT_{max} and (c) maximum azimuthally-averaged tangential wind component V_{max} at 900mb.

After initialization at 00:00 UTC 26 Jan, the vortex in all the MM5 calculations undergoes an adjustment phase in which V_{max} decays slightly during the first hour, before intensifying rapidly over the next two hours and then decaying over a further six hours to a value close to that in the ECMWF analysis, about 11 m s^{-1}. Following this adjustment phase, V_{max} remains approximately steady in

[§]In the MM5 model, the bucket soil moisture scheme keeps a budget of soil moisture allowing moisture availability to vary with time, particularly in response to rainfall and evaporation rates. (Dudhia et al. 2005, pp8-15)

[¶]An alternative definition of the vortex centre might be the location of minimum total wind speed at some low level and within some radius of the minimum sea-level pressure centre. However, it was found that the locations of the minimum sea-level pressure and minimum absolute wind at 900 mb are mostly within 10 km of each other

Symbol	Description
C0	Control experiment using the default M_a values in summer
C1	As C0, except that the initial value of M_a is decreased by 20%
C2	As C0, except that the initial value of M_a is decreased by 10%
C3	As C0, except that the initial value of M_a is increased by 10%
C4	As C0, except that the initial value of M_a is increased by 20%
C5	As C0, except that the initial value of M_a is increased by 50%
C6	As C0, except that M_a is not allowed to vary with time in response to rainfall and evaporation rates

Table I. Control and six sensitivity simulations

both the MM5 model and in the ECMWF analyses for a period of about 12 h before increasing gradually during 27 Jan to reach about 15 m s^{-1}. The initial decay is not seen in the VT_{max} curves, which are indicative of local rather than azimuthally-averaged conditions. After the initial adjustment phase, the agreement of the V_{max} values between the MM5 simulations and the ECMWF analyses is remarkably good. As would be expected, the agreement is not so good when judged in terms of VT_{max}, a result that is expected because of the higher horizontal resolution of the MM5 calculations. The significantly higher values of VT_{max} in the MM5 calculations are consistent with the idea that the higher resolution enables convective features to be better represented and less smeared out than in the ECMWF analyses. The grid spacing in ECMWF analyses is 0.125^o (approximately 13 km) while in the MM5 model it is only 3 km for the inner domain.

A significant finding is that there is no systematic difference in the behaviour of VT_{max} and V_{max} between experiments C0 and C6, indicating that the along-track rainfall has a minimal positive impact in terms of vortex intensity. This result is presumably because the rainfall across the vortex is patchy and doesn't contribute appreciably to surface moisture fluxes (see section 7). The finding is in line with that of Evans et al. (2011) for Tropical Storm Erin (2007), but does not support the hypothesis of Emanuel et al. (2008), who suggest that the along-track rainfall is a significant factor in the overland re-intensification of tropical cyclones over Australia. There is little sensitivity of the VT_{max} and V_{max} values to the initial value of M_a in the MM5 simulations on the first day of integration, but the differences become larger (by 10% to 30%) on the second day. These differences may be attributed to a stochastic element in the patterns of deep convection as examined later in section 6. In general, the values of P_{min} and V_{max} for all MM5 simulations fit those in the ECMWF analyses well.

4.2. *Evolution of vertical velocity and relative vorticity*

The left panels of Fig. 5 show patterns of the vertical velocity at 500 mb in the control experiment C0 at selected times. The right panels show the corresponding patterns of the vertical component of relative vorticity at 850 mb with the storm-relative wind vectors at this level superimposed. The system translation velocity is based on the movement of the vortex centre as defined in section 4.1. The top two panels show the situation at 03:00 UTC 26 Jan during the initial period of rapid intensification. At this time, deep convection is evident in the pattern of vertical velocity which has several strong irregularly-spaced updraught cores with vertical velocities up to 11 m s^{-1}. Significantly, one updraught complex straddles the centre of circulation, a feature that is particularly conducive to vortex spin up by the conventional spin up mechanism as discussed in the next section. The updraught cores are approximately colocated with regions of significantly enhanced vertical vorticity indicative of the stretching of system-scale cyclonic vorticity by the updraughts (Hendricks et al. 2004; Montgomery et al. 2006; Kilroy and Smith 2013; Kilroy et al. 2014; Kilroy and Smith 2015). Hendricks et al. (2004) referred to these vortical updraughts as "Vortical Hot Towers".

Three hours later, at 06:00 UTC (15:30 CST[‖]), deep convection has collapsed within 50 km radius of the circulation centre (Fig. 5c) although a region of enhanced relative vorticity remains around this centre (Fig. 5d). Soon after 08:00 UTC 27 Jan, the vortex undergoes two brief periods of intensification each lasting 1-2 hours (see blue curve in Fig. 4c). As on the previous day, the existence of these periods coincides with the reappearance of deep convective cells near the centre of circulation as exemplified by the vertical motion field at 08:00 UTC shown in Fig. 5e. The two cells closest to the storm centre of circulation are accompanied by regions of enhanced vertical vorticity as seen in Fig. 5f. These cells of deep convection do not survive over a diurnal cycle: indeed by 18:00 UTC 27 Jan (03:30 CST 28 Jan), when the vortex intensity has reached a local maximum ($V_{max} \approx 15$ m s^{-1}), there are no strong updraughts within a radius of some 90 km of the circulation centre. Six hours after this time the vortex begins a period of decay.

5. Dynamics of spin up

The spin up described in the previous subsection involves dynamical processes that are intrinsically asymmetric, although one can examine the dynamics of spin up from an axisymmetric perspective by azimuthally averaging the flow fields. In this perspective, departures from axial symmetry in the mean momentum equations appear as "eddy terms" (Persing et al. 2013; Smith et al. 2015b). In this section we examine the basic dynamics of vortex spin up in an axisymmetric framework and in section 7 we investigate aspects of the thermodynamic support for spin up. The primary focus here will be on the tangential wind component, v, as well as the surfaces of absolute angular momentum, M, henceforth referred to as the M-surfaces, which are derived from this component. The quantity, M is defined as

$$M = r < v > + \frac{1}{2} f r^2, \qquad (1)$$

[‖] Central Standard Time = UTC + 9h 30 min

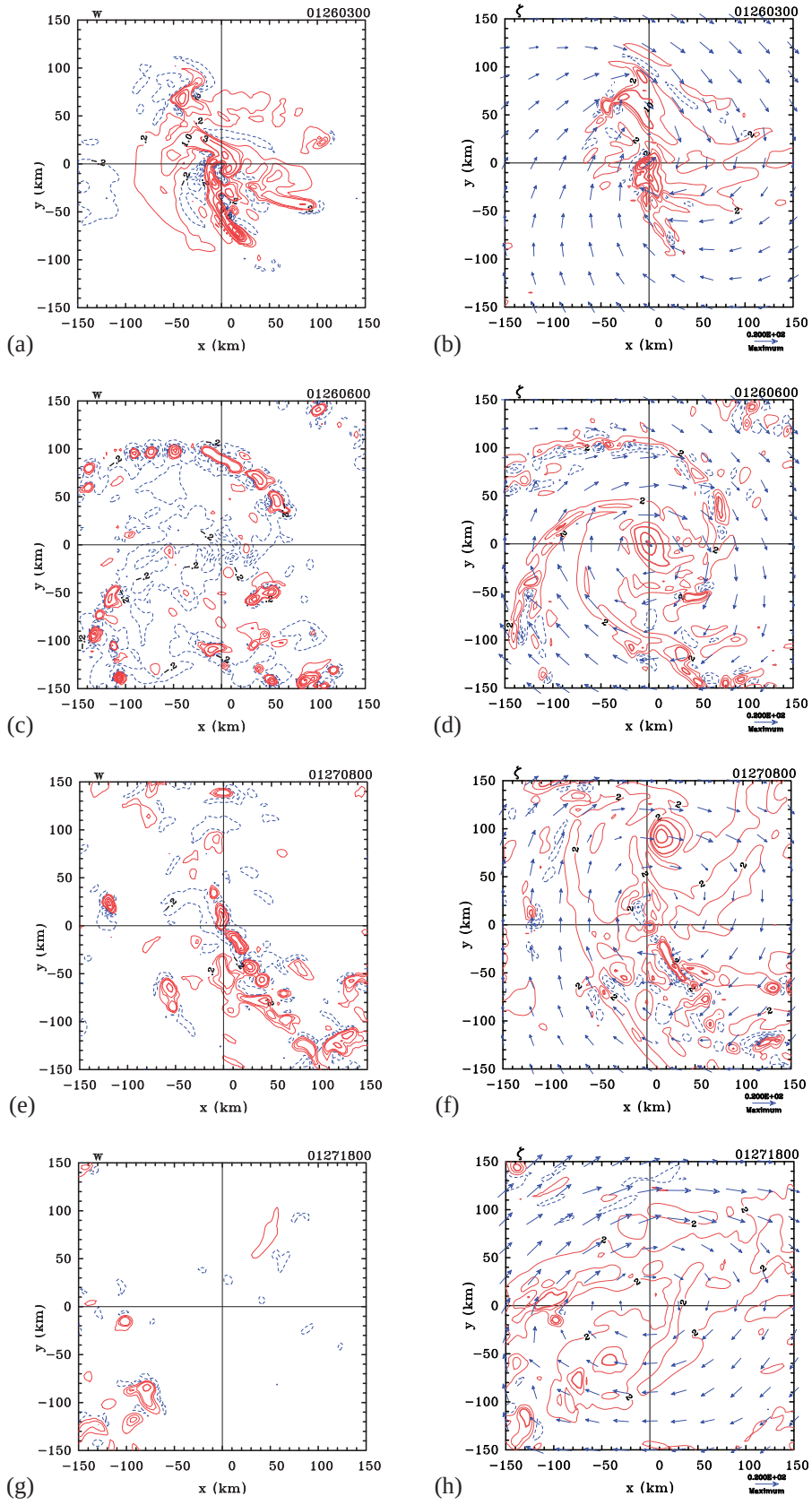

Figure 5. Vertical velocity at 500 mb (left panels) and the relative vertical vorticity at 850 mb with the storm-relative wind vectors superimposed (right panels) at 03:00, 06:00 UTC 26 Jan and 08:00, 18:00 UTC 27 Jan in the control experiment C0. Contour interval for vertical velocity: thick curves 2.0 ms^{-1} and thin curves 0.4 m s^{-1} with highest absolute value 1.0 m s^{-1}. Contour interval for relative vorticity: thick curves 10×10^{-4} s^{-1} and thin curves 4×10^{-4} s^{-1} with highest absolute value 6×10^{-4} s^{-1}. Cyclonic (negative) values are solid curves in red and anticyclonic (positive) values are dashed curves in blue.

where r is the radius from the vortex centre, $< v >$ is the azimuthally-averaged tangential wind speed, and f is the Coriolis parameter, assumed to be a constant.

Inspection of Fig. 5 suggests that the $< v >$ and M-fields may have a higher degree of axial symmetry than,

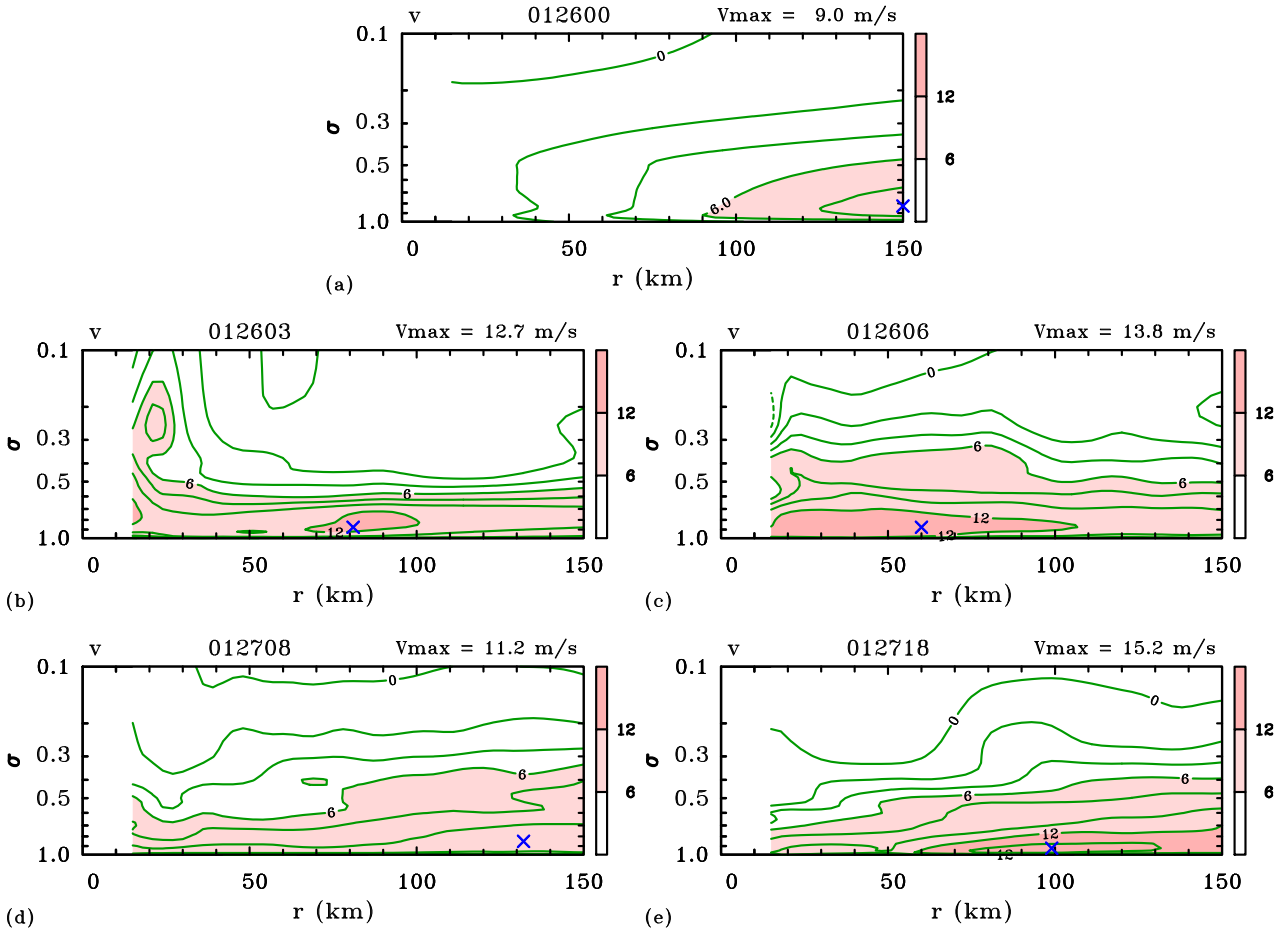

Figure 6. Radius-height cross-section of isotachs of azimuthally-averaged tangential wind at (a) 00:00, (b) 03:00, (c) 06:00 UTC 26 Jan and (d) 08:00, (e) 18:00 UTC 27 Jan in the control experiment. Contour interval 2 m s^{-1}. Cyclonic (negative) values are solid curves and anticyclonic (positive) values are dashed curves. The X symbol marks the position of the maximum azimuthally-averaged tangential wind.

for example, the vertical velocity and relative vorticity. We show also the azimuthally-averaged radial wind component, but caution that this may be more prone to error than the tangential component because any error in the centre finding procedure can lead to aliasing of the tangential wind component into the radial component**.

Figure 6 shows radius-height plots of $< v >$ in the control experiment at the initial time and at same times as in Fig. 5. At the initial time, 00:00 UTC 26 Jan (Fig. 5a), there is a monotonic increase in $< v >$ out to 150 km, the maximum radius shown, and the maximum $< v >$ (9 m s^{-1}) occurs at about σ = 0.8 (on the order of 2 km height). Three hours later, at 03:00 UTC (Fig. 5b), the winds at low levels have increased with two prominent local maxima, one at a radius of about 15 km and the other at a radius of about 80 km. both being a little over 12 m s^{-1}. Inspection of Fig. 5a suggests that the low-level spin up is associated with the early development of deep convection near the circulation centre and that the local maximum of $< v >$ is associated with the convective cell at the axis. Three hours later, at 06:00 UTC (Fig. 6c), the vortex has strengthened in depth, but the maximum $< v >$ has increased only slightly. In fact, Fig. 4 shows that the intensity of the vortex is on the decline at this time, which is near the end of the initial adjustment period. This decline continues for about another three hours after which the intensity begins to slowly increase. Nevertheless, at 08:00 UTC 27 Jan (Fig. 6d), the vortex is still a little weaker and shallower than at 06:00 UTC on the previous day.

The increase in intensity is most marked during the following 10 hours, the maximum $< v >$ increasing by about 4 m s^{-1} to 15.2 m s^{-1} (Fig. 6e). Even so, the maximum $< v >$ is located at a radius of 100 km from the storm centre at this time. It is noteworthy that this maximum occurs always at low levels with values of σ exceeding 0.8, corresponding with heights of approximately 2 km or less.

Figure 7 shows radius-height plots of the azimuthally-averaged radial velocity superimposed on the M-surfaces at the same times as those in Fig. 6. Values of M less than 4×10^5 m^2 s^{-1} are highlighted in blue to represent some inner core region, and those larger than 1×10^6 m^2 s^{-1} are highlighted in red in Fig. 7 to represent some outer core region.

Prominent structural features are that, in the lower troposphere, at least for values of σ exceeding 0.5, M increases with radius at each level at each time, implying that the vortex is centrifugally (or inertially) stable (e.g. Shapiro and Montgomery 1993; Franklin et al. 1993); and that the M-surfaces slope inwards with decreasing radius within the boundary layer and outwards with radius aloft.

**An estimate of error in the radial wind due to error in the centre finding has been carried out by moving the centre 15 km northward, southward, eastward, and westward in the control experiment. It was found that the time-averaged error in the radial wind within a radius of 15 km of the centre can be as large as 90%, but the error falls rapidly to less than 25% beyond this radius.

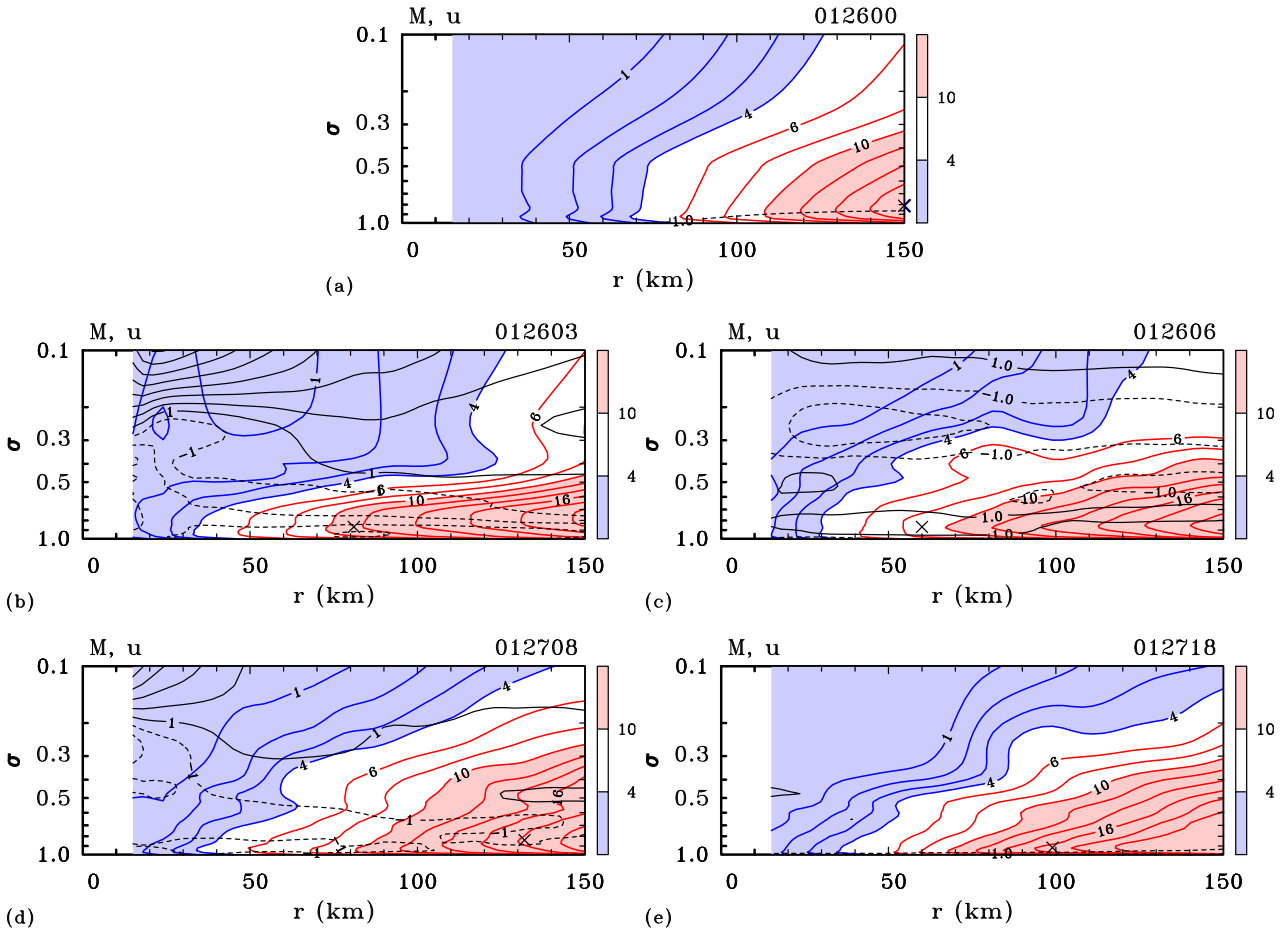

Figure 7. Radius-height cross-section showing contours of azimuthally-averaged radial velocity and the magnitude of the absolute angular momentum at (a) 00:00, (b) 03:00, (c) 06:00 UTC 26 Jan and (e) 08:00, (f) 18:00 UTC 27 Jan in the control experiment. Contour interval for absolute angular momentum: blue curves 1×10^5 m^2 s^{-1} with highest value 4×10^5 m^2 s^{-1}; red curves 2×10^5 m^2 s^{-1}. Contour interval for radial velocity is 2 m s^{-1}, positive values are solid curves and negative values are dashed curves. The X symbol marks the position of the maximum azimuthally-averaged tangential wind.

These slopes give rise to a nose-like feature near the top of the boundary layer. As explained in Smith et al. (2015b, see their section 7.1), this structure of the M-surfaces may be understood as follows. Above the boundary layer, $< v >$ is close to gradient wind balance and thermal wind balance. Thus, because the tropical cyclone vortex is warm cored, the M-surfaces lean outwards there. The inward-slope of the M-surfaces near the surface is manifestation of the reduction of $< v >$ and hence M by the frictional torque at the surface and the corresponding turbulent diffusion of $< v >$ to the surface.

The figure shows also that during periods of intensification, the M-surfaces in the low to mid troposphere move radially inwards so that the tangential winds are amplified (because $< v >= M/r - \frac{1}{2}fr$). In the upper troposphere, the M surfaces move radially outwards. As discussed in section 4.2, the periods of intensification are associated with the development of deep convection near the circulation centre. The collective effects of this convection generate an overturning circulation with inflow in the lower troposphere that converges the M-surfaces above the boundary layer, where to a first approximation, M is materially conserved. In contrast, during the period of decay between 03:00 UTC and 06:00 UTC 26 Jan, the pattern of inflow and outflow are reversed, as is the radial movement of the angular momentum surfaces in the upper and lower troposphere.

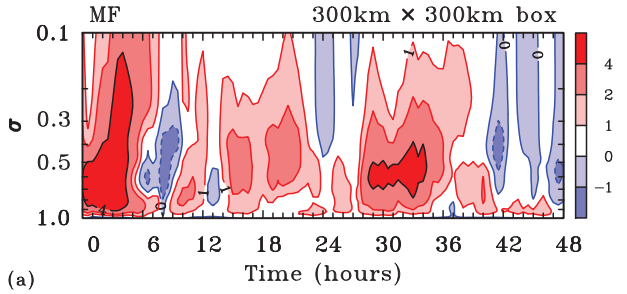

Figure 8. Time-height cross sections of the vertical mass flux per unit area (Unit: 10^{-2} kg m^{-2} s^{-1}) within a box 300 km × 300 km centred on the location of the minimum sea-level pressure in the control experiment. Time zero corresponds to the start of the simulation at 00:00 UTC 26 Jan.

Figure 8 shows time-height cross sections of the vertical mass flux ρw, averaged over a square box 300 km × 300 km centred on the location of the minimum sea-level pressure in the control experiment. Here, ρ is the density and w is the vertical velocity. Notable features of the mass flux within the box are two "bursts" centred at 03:00 UTC 26 Jan (3 h in the figure) and 08:00 UTC 27 Jan (32 h in the figure). Interestingly, the two bursts are each accompanied by an increase of the maximum tangential wind speed (Fig. 4c). These bursts are not obviously related to the diurnal cycle of convection over land.

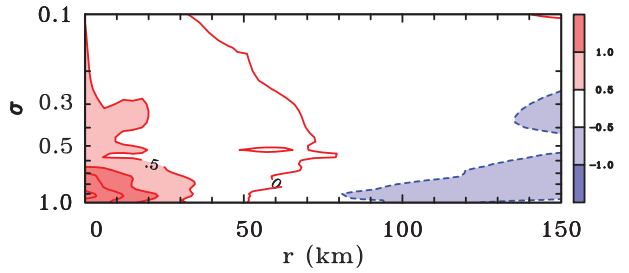

Figure 9. Radius-height cross-section of the azimuthally-averaged potential temperature anomaly from the areal mean (unit: K), time averaged during the period of rapid intensification from 05:00 to 11:00 UTC 27 Jan in the control simulation.

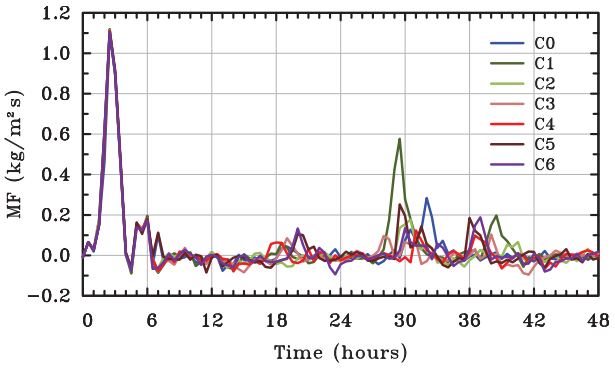

Figure 10. Time series of the area-averaged vertical mass flux within a radius of 30 km from the centre at 500 mb for all sensitivity simulations. Time zero corresponds to the start of each simulation at 00:00 UTC 26 Jan.

The foregoing results are similar to those found for an idealized tropical cyclone by Smith et al. (2009) and in observations and simulations of a major hurricane (Evans et al. 2011; Montgomery et al. 2014; Smith et al. 2015b), suggesting that the intensification mechanism of tropical lows over land is similar to that of tropical cyclones. Perhaps the main difference is the much weaker radial inflow in the low studied here suggesting that the boundary layer control on convection (Kilroy et al. 2016) is much less than in a tropical cyclone.

In contrast to the similarities with tropical cyclones over the sea, the azimuthally averaged thermal structure shown in Fig. 9 would appear to be somewhat different. While the system is warm cored, the maximum potential temperature anomaly is found in the lower troposphere rather than in the middle to upper troposphere as is usual in tropical cyclones. It turns out, however, that because of weak vertical shear, the thermal anomaly in the mid to upper troposphere (pressures 500 mb and lower) is displaced by several tens of kilometres to the southwest relative to that at low levels and may be concealed by the azimuthal averaging about a vertical axis. Even so, horizontal plots of potential temperature at each height (not shown) indicate that the maximum azimuthally-averaged potential temperature anomaly is still located in the lower troposphere rather than mid or upper troposphere. This feature is consistent with the fact that the vertical shear of the tangential wind is a maximum in the lower troposphere (Fig. 6).

6. Sensitivity simulations

Referring back to Fig. 4, the sensitivity simulations in which the initial moisture availability is varied indicated little sensitivity of P_{min}, VT_{max} and V_{max} on the first day of integration, but significant differences in behaviour emerge on the second day. The reasons for these differences are examined now.

The curves for V_{max} in experiments C1, C2, C0 and C5 show sharp increases at approximately 06:00, 06:00, 08:00 and 12:00 UTC 27 Jan, respectively (Fig. 4c), indicating a brief period of rapid spin up near these times. In contrast, there are no such periods in the other two simulations C3 and C4. The differences in behaviour between these two sets of simulations are a reflection of the stochastic nature of deep convection and may be understood in terms of the classical mechanism for spin up (Ooyama 1969; see also Montgomery and Smith 2014). From an azimuthally-averaged perspective, the spin up of the mean tangential winds above the boundary layer occurs as a result of the convectively-induced inflow of air towards the circulation centre. If convection develops near the centre of the circulation, the inflow it produces draws the M-surfaces inwards and, since M is materially conserved there, the tangential wind increases as described in section 5.

Figure. 10 shows time series of the area-averaged vertical mass flux (MF) within a radius of 30 km from the centre at 500 mb for all sensitivity simulations. In each case, the variation of MF is, to some extent, similar to that of V_{max} in Fig. 4c, supporting the idea that the occurrence of convection near the centre of the circulation is a key requirement for the spin up of the azimuthally-averaged tangential winds. It may be significant that only the experiments whose MF values become close or exceed 0.2 on 27 Jan undergo a burst of rapid intensification. The peak values of MF for C1 are up to 0.6 and 0.2 at approximately 05:30 and 15:00 on 27 Jan, respectively. It is at approximately the same time that V_{max} shows sharp increases. Similarly, the curves for V_{max} in experiments C2, C0 and C5 show sharp increases at approximately the same time that their MF values are close to or greater than 0.2. In contrast, in experiments C3 and C4, where the MF values are much smaller than 0.2, V_{max} does not show any burst of rapid intensification.

Figure 11 shows the vertical velocity at 500 mb together with horizontal wind vectors at 850 mb at times corresponding approximately with the brief times of rapid intensification in experiments C1, C2, C0 and C5 on 27 Jan (panels a-d). This figure shows also two arbitrarily chosen snapshots in experiments C3 and C4 (panels e-f) at the foregoing times. In experiments C1, C2, C0 and C5 there are convective updraughts at and near the circulation centre. For example, in experiments C1 and C2 at 06:00 UTC 27 Jan, there are updraughts within a radius of 10-20 km of the vortex centre with a maximum speeds of approximately 7 m s^{-1} (Fig. 11a and Fig. 11b, respectively). In contrast, in experiment C4 (Fig. 11e) the strongest updraughts are approximately 150 km to the northwest of the vortex centre, again with vertical velocity maxima of 7 m s^{-1}. There is just one updraught with a maximum velocity a little over 1 m s^{-1} about 50 km west-southwest of the vortex centre.

At 08:00 UTC 27 Jan in experiment C0 (Fig. 11c), there is an updraught extending northwards from the centre and another one extending 30 km to the southeast. These have vertical velocities up to 5 m s^{-1} and 7 m s^{-1}, respectively. At the same time, in experiment C3, the nearest significant updraughts lie at a radius of about 40 km from the centre

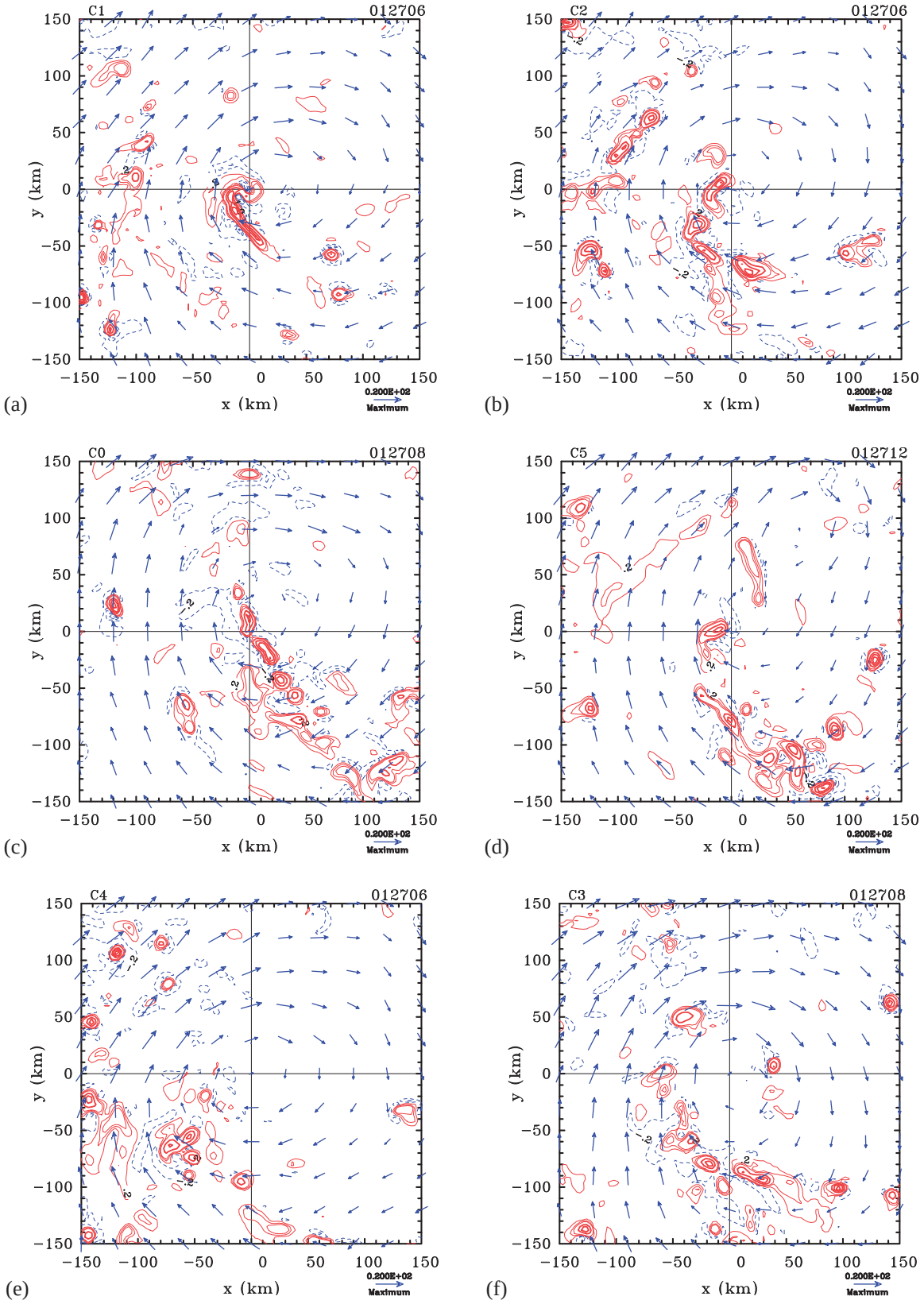

Figure 11. Vertical velocity at 500 mb together with wind vectors at 850 mb for (a) experiment C1, and (b) experiment C2 at 06:00 UTC 27 Jan; (c) experiment C0 at 08:00 UTC 27 Jan; (d) experiment C5 at 12:00 UTC 27 Jan; (e) experiment C4 at 06:00 UTC 27 Jan; (f) experiment C3 at 08:00 UTC 27 Jan. Contour interval: thick curves 2.0 m s^{-1} and thin curves 0.4 m s^{-1} with highest absolute value 1.0 m s^{-1}. Positive values are solid curves in red and negative values are dashed curves in blue.

(Fig. 11f). In experiment C5 at 12:00 UTC 27 Jan, there is an updraught with a velocity maximum of about 5 m s^{-1} located 10 km to the west of the vortex centre (Fig. 11d).

In summary, the vortices in each of the experiments C1, C2, C0 and C5 have pulses of intensification that are accompanied by strong convective updraughts near the circulation centre. In experiments C3 and C4, there

are no such pulses and at no time do significant strength updraughts develop near the vortex centre. These results suggest the hypothesis that only the vortices that have deep convection near their centre of circulation will undergo pulses of rapid intensification. The results add further support for the idea that a key requirement for the intensification of storms in general is the occurrence of deep convection near or at the existing centre of circulation. This result accords with the findings of Smith et al. (2015a) and Kilroy et al. (2015). The requirement transcends earlier ideas invoking the increased efficiency of diabatic heating in the high inertial stability region of the vortex core (e.g. Schubert and Hack 1982; Hack and Schubert 1986; Vigh and Schubert 2009) for reasons articulated in a recent paper by Smith and Montgomery (2015a). In essence, the most effective spin up requires M-surfaces to be drawn inwards to small radii. Geometrically speaking, convection located at a given radius can only draw air inwards outside that radius. Inside that radius, air will be drawn outwards. Thus, inside the convection radius, M-surfaces will be drawn outwards with a consequent spin down there. In spite of the fact that the large inertial stability at small radii will oppose the inward displacement of the M-surfaces, only convection located near the circulation centre is able to draw the M-surfaces inwards to small radii to spin up the tangential circulation above the frictional boundary layer as discussed in section 5. Note, the inflow in the vortices under study here is sufficiently weak (Figure 7) that the boundary layer control ideas discussed by Kilroy et al. (2016) are only minimally operative.

The significant differences in the patterns of vertical velocity fields for the different sensitivity simulations in Fig. 11 highlight the stochastic variability of deep convection resulting from the differences in the initial moisture availability and, as shown above, this variability adds a stochastic element to the intensification process itself, consistent with the results of Nguyen et al. (2008) and Shin and Smith (2008).

7. Thermodynamic support for spin up

In the two previous sections we have presented evidence in support of Evans et al. (2011)'s speculation noted in the Introduction that the development and organization of deep moist convection near the centre of the vortex is necessary for vortex intensification to occur. The question remains, however, where does the moisture come from to support sustained deep convection near the vortex centre over land? In particular, how important are surface moisture fluxes compared to the horizontal advection of moisture in maintaining deep convection? In a model simulation such as ours that captures the intensification of a low over land, it should be possible to address these questions by way of a moisture budget analysis of the model output.

We examine now the importance of surface evaporation compared with the horizontal transport of moisture into the system. A simple moisture budget for a vertical column of unit horizontal cross-section is given by:

$$\frac{\partial TPW}{\partial t} = E - P + S, \qquad (2)$$

where $\partial TPW/\partial t$ is the change in total precipitable water (TPW) with time, E is the rate of evaporation of moisture from the surface, P is rate of moisture loss by precipitation

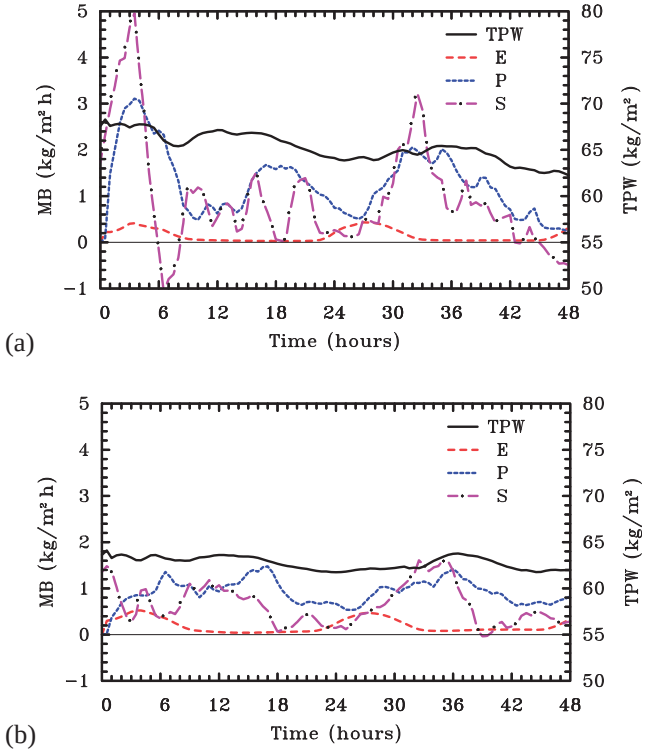

Figure 12. Sources and sinks of moisture including the contributions by surface evaporation (E), precipitation (P) and the horizontal transport of moisture (S) in Eq. (2) averaged over boxes: (a) 300 km × 300 km, (b) 600 km × 600 km centred on the location of the minimum sea-level pressure in the control experiment. Shown also is the total precipitable water (TPW) in kg m^{-2}. Time zero corresponds to the start of the simulation at 00:00 UTC 26 Jan.

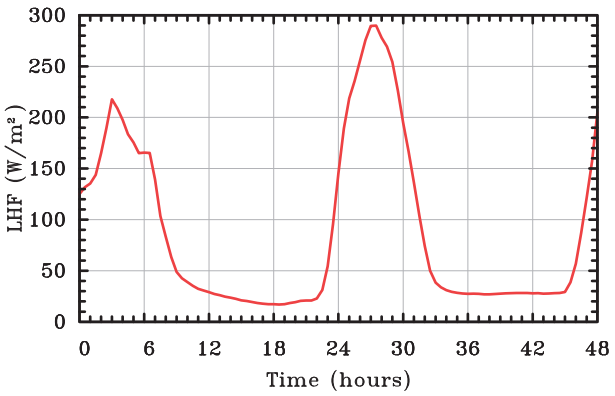

Figure 13. Time series of the area-averaged surface latent heat flux within a radius of 150 km from the centre in the control experiment. Time zero corresponds to the start of the simulation at 00:00 UTC 26 Jan.

and S is the rate of moisture convergence through the sides of the column. Moisture convergence is calculated by vertically integrating the fluxes of moisture into a box centred on the system. These three quantities are then averaged over the area of the box to provide units of kg m^{-2} h^{-1}.

Figure 12 shows time series of terms in the moisture budget for the control simulation, C0, for two columnar regions extending to the model top. One column has a horizontal cross section 300 km × 300 km square centred on the vortex centre and the other has a 600 km × 600 km square cross section. The terms include: the contributions to the box-averaged moisture tendency by surface evaporation (E), precipitation (P), and the horizontal transport of

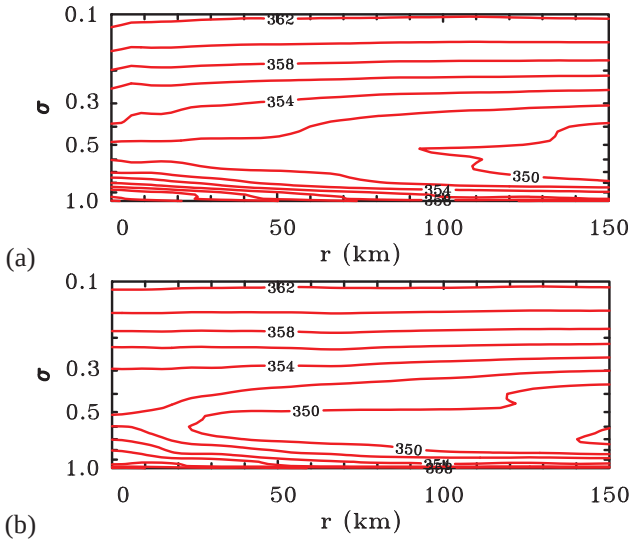

Figure 14. (a) Radius-height cross-section of the azimuthally-averaged pseudo-equivalent potential temperature (unit: K), time averaged during the period of rapid intensification from 05:00 to 11:00 UTC 27 Jan in the control experiment. (b) A similar cross-section for Expt. C6 during the same time period.

moisture through the sides of the column (i.e. S). Shown also is the total precipitable water (TPW) averaged over the column. Figure 12 shows that, at most times, the flux of moisture into the sides of these two columnar regions is approximately equal to the amount of moisture lost by precipitation, while the contribution from the mean surface evaporation is small in comparison. Notwithstanding the fact that the budget does not close because water substance is not strictly a conserved quantity in MM5 (Braun 2006), a similar result has been found also for tropical cyclones (e.g. Kurihara 1975; Braun 2006; Trenberth et al. 2007).

Focussing first on the 300 km $\times$ 300 km square column (Fig. 12a), there is a steady decline in mean TPW from an initial value of 68 kg m^{-2} to about 62 kg m^{-2} at the end of the 48 h simulation. These are relatively large values, but typical of the Australian monsoon regime (see e.g. Kilroy et al. 2015). For comparison, observed values found in the "pouch" regions of pre-genesis Atlantic and Carribean wave disturbances during the PREDICT experiment (Montgomery et al. 2012) were generally around 60 kg m^{-2} near the sweet spot of the pouch (values for Tropical Storm Gaston are shown in Figs. 2 and 3 of Smith and Montgomery (2010)). Mean values of TPW in monsoonal flow conditions at Darwin are typically about 57 kg m^{-2} (Črnivec and Smith 2016). There are large fluctuations in S and P during the early adjustment period (the first 8 h of the simulation), but these have a relatively small net effect on the mean TPW change. After the adjustment phase, there are two broad peaks in precipitation, one centred around 19:00 UTC 26 Jan and the other around 08:00 UTC 27 Jan. Not surprisingly, these peaks coincide approximately with similar peaks in the vertical mass flux shown in Fig. 8, but they are not obviously related to peaks in E, which have a clear diurnal signal.

A similar behaviour of terms in the moisture budget for the 600 km $\times$ 600 km square column is seen in Fig. 12b, but the magnitude of the fluctuations is smaller, especially during the adjustment period.

Figure 13 shows time series of latent heat flux averaged within a radius of 150 km from the centre in the control experiment. The curve mimics closely the behaviour of the curve for E in Fig. 12, but is multiplied by the coefficient of latent heat to give units of W m^{-2}. Again the diurnal signal is a prominent feature with peak values at about 03:00 UTC on the order of 300 W m^{-2}. However, the mean value averaged over a day is appreciably smaller, 103 W m^{-2}, a value close to that found by (Evans et al. 2011, p. 3860) for large areas of Tropical Storm Erin. Despite the smallness of the surface moisture fluxes in the overall moisture budget, one should not conclude that these fluxes are unimportant.

Figure 14a shows a radius-height cross section of pseudo-equivalent potential temperature, θ_e, in the control experiment, time averaged during the period of rapid intensification from 05:00 to 11:00 UTC 27 Jan. The Emanuel theory for vortex intensification predicts substantially elevated values of θ_e in the vortex core (e.g. Emanuel 1989). In the theory, these are tied to an increase in the surface enthalpy fluxes accompanying an increase in the surface wind speed with decreasing radius. There are, indeed, elevated values of θ_e in a shallow layer near the surface, but the corresponding (negative) radial gradient is weak in the middle troposphere, unlike that envisaged in the Emanuel theory for vortex intensification in an axisymmetric model (see e.g. Fig. 9.15b in Holton 2004). However, the elevated values of θ_e near the surface contribute to the conditional instability of air in the inner region of the vortex. The need for such elevated values of θ_e for a tropical cyclone to intensify was first pointed out by Malkus and Riehl (1960).

Figure 14b shows a similar cross section of θ_e in experiment C6 in which the coupling between rainfall and moisture availability is suppressed. Again, near-surface θ_e values are elevated near the vortex centre, but not so much as in the control experiment. Thus, even in this case, surface fluxes act to support local conditional instability near the vortex centre.

In summary, we have shown that the horizontal transport of moisture into a mesoscale box following the low is essentially equal to the moisture lost by precipitation. The contribution to the moisture budget by surface fluxes is small in comparison. Nevertheless, the small moisture fluxes play an important role in generating convective instability in a monsoon environment that already has relatively high values of TPW so that deep convective bursts can continue to occur even when the system is located far inland.

8. Conclusions

We have analysed the intensification of tropical low over land in numerical simulations of an event that occurred over northern Australia in January 2006 during the TWP-ICE experiment. A control simulation together with a series of five sensitivity simulations were discussed. The sensitivity simulations were determined by varying the initial moisture availability from that in the control calculation, a procedure that adds, *inter alia*, a stochastic element to the development and evolution of deep convection. In one further simulation, the coupling between moisture availability and model-produced precipitation was suppressed. The results of the simulations were interpreted in terms of the classical axisymmetric paradigm for tropical cyclone intensification with recent modifications.

The spin up of the low over land is shown to be favoured by the development of deep convection near the centre of

the circulation, which is initially weak. This convection leads to an overturning (in, up and out) circulation that draws absolute angular momentum surfaces inwards in the lower troposphere leading to spin up of the azimuthally-averaged tangential winds above the boundary layer. In this respect, the intensification process is similar to that for tropical cyclones over sea. The intensification takes place within a moist monsoonal environment, which is evidently sufficient to support sporadic deep convection within the low's circulation. A moisture budget for two mesoscale columns of air encompassing the low show that the horizontal import of moisture is roughly equal to the moisture lost by precipitation whereas surface moisture fluxes make only a small contribution to the overall budget. Nevertheless, enhanced surface moisture fluxes near the circulation centre play an important role in supporting deep convection and thereby the intensification process. The evolution of the simulated low was largely unaffected when the coupling between rainfall and moisture availability was suppressed. This is presumably the case because the rainfall is patchy across the vortex.

Acknowledgement

We are grateful to our colleague Gerard Kilroy, who gave generous help to the first author in setting up and running the MM5 model. We are grateful also to Hongyan Zhu and an anonymous reviewer for their constructive comments on the original version of the submitted manuscript. ST and MG gratefully acknowledge financial supports for this research from the National Natural Science Foundation of China (91215302, 90715040), Key project of State Key Lab. of Disaster Reduction in Civil Eng. (SLDRCE15-A-04), RKS acknowledges support from the German Research Council (Deutsche Forschungsgemeinschaft) under Grant number SM30-23 and the Office of Naval Research Global under Grant No. N62909-15-1-N021. MTM acknowledges the support of NSF grant AGS-1313948, NOAA HFIP grant N0017315WR00048, NASA grant NNG11PK021 and the U. S. Naval Postgraduate School..

References

Arndt, D. S., J. B. Basara, R. A. McPherson, B. G. Illston, G. D. McManus, and D. B. Demkos, 2009: Observations of the reintensification of Tropical Storm Erin (2007). *Bull. Amer. Meteor. Soc.*, **99**, 1079–1093, doi:10.1175/2009BAMS2644.1.

Braun, S. A., 2006: High-resolution simulation of Hurricane Bonnie (1968). Part II: Water budget. *J. Atmos. Sci.*, **63**, 43–64.

Brennan, M. J., R. D. Knabb, M. Mainelle, and T. B. Kimberlain, 2009: Atlantic hurricane season of 2007. *Mon. Wea. Rev.*, **137**, 4061–4088.

Bui, H. H., R. K. Smith, M. T. Montgomery, and J. Peng, 2009: Balanced and unbalanced aspects of tropical-cyclone intensification. *Quart. Journ. Roy. Meteor. Soc.*, **135**, 1715–1731.

Davidson, N. E. and G. H. Holland, 1987: A diagnostic analysis of two intense monsoon depressions over Australia. *Mon. Wea. Rev.*, **115**, 380–392.

Dudhia, J., 1993: A non-hydrostatic version of the Penn State/NCAR mesoscale model: Validation tests and simulation of an Atlantic cyclone and cold front. *Mon. Wea. Rev.*, **121**, 1493–1513.

Dudhia, J., D. Gill, K. Manning, W. Wang, and C. Bruyere, 2005: *PSU/NCAR Mesoscale Modeling System Tutorial Class Notes and User's Guide: MM5 Modeling System Version 3*. [Available online at http://www2.mmm.ucar.edu/mm5/documents/tutorial-v3-notes.html].

Dunkerton, T. J., M. T. Montgomery, and Z. Wang, 2009: Tropical cyclogenesis in a tropical wave critical layer: easterly waves. *Atmos. Chem. Phys.*, **9**, 5587–5646.

Eckel, T., 2002: *Perturbing MM5 Moisture Availability for Ensemble Forecasting*. [Available online at http://www.atmos.washington.edu/~ens/pdf/ATMS547_JUN2002.teckel.pdf].

Emanuel, K., J. Callaghan, and P. Otto, 2008: A hypothesis for the redevelopment of warm-core cyclones over northern Australia. *Mon. Wea. Rev.*, **136**, 3863–3872.

Emanuel, K. A., 1989: The finite amplitude nature of tropical cyclogenesis. *J. Atmos. Sci.*, **46**, 3431–3456.

Evans, C., R. S. Schumacher, and T. J. Galarneau, 2011: Sensitivity in the overland reintensification of Tropical Cyclone Erin (2007) to near soil moisture characteristics. *Mon. Wea. Rev.*, **139**, 3848–3870.

Fang, J. and F. Zhang, 2010: Initial development and genesis of Hurricane Dolly (2008). *J. Atmos. Sci.*, **67**, 655–672.

Foster, I. J. and T. J. Lyons, 1984: Tropical cyclogenesis: A comparative study of two depressions in the northwest of Australia. *Quart. Journ. Roy. Meteor. Soc.*, **110**, 105–119.

Franklin, J. L., S. J. Lord, S. E. Feuer, and F. D. Marks, 1993: The kinematic structure of Hurricane Gloria (1985) determined from nested analyses of dropwindsonde and Doppler radar data. *Mon. Wea. Rev.*, **121**, 2433–2451.

Grell, G. A., J. Dudhia, and D. R. Stauffer, 1995: A description of the fifth generation Penn State/NCAR mesoscale model (MM5). *NCAR Tech Note NCAR/TN-398+STR.*, **000**, 138.

Hack, J. J. and W. H. Schubert, 1986: Nonlinear response of atmospheric vortices to heating by organized cumulus convection. *J. Atmos. Sci.*, **43**, 1559–1573.

Hendricks, E. A., M. T. Montgomery, and C. A. Davis, 2004: The role of "vortical" hot towers in the formation of Tropical Cyclone Diana (1984). *J. Atmos. Sci.*, **61**, 1209–1232.

Holton, J. R., 2004: *An Introduction to Dynamic Meteorology (4th Edn.)*. Elsevier Academic Press., 535 pp.

Hong, S. Y. and H. L. Pan, 1996: Nonlocal boundary layer vertical diffusion in a medium-range forecast model. *Mon. Wea. Rev.*, **124**, 2322–2339.

Kilroy, G. and R. K. Smith, 2013: A numerical study of rotating convection during tropical cyclogenesis. *Quart. Journ. Roy. Meteor. Soc.*, **139**, 1255–1269.

— 2015: Tropical-cyclone convection: the effects of a vortex boundary layer wind profile on deep convection. *Quart. Journ. Roy. Meteor. Soc.*, **141**, in press.

Kilroy, G., R. K. Smith, and M. T. Montgomery, 2016: Why do model tropical cyclones grow progressively in size and decay in intensity after reaching maturity? *J. Atmos. Sci.*, **72**, 487–503.

Kilroy, G., R. K. Smith, M. T. Montgomery, B. Lynch, and C. Earl-Spurr, 2015: A case study of a monsoon low that intensified over land as seen in the ECMWF analyses. *Quart. Journ. Roy. Meteor. Soc.*, **141**, submitted.

Kilroy, G., R. K. Smith, and U. Wissmeier, 2014: Tropical cyclone convection: the effects of ambient vertical and horizontal vorticity. *Quart. Journ. Roy. Meteor. Soc.*, **140**, 1756–1177.

Kurihara, Y., 1975: Budget analysis of a tropical cyclone simulated in an axisymmetric numerical model. *J. Atmos. Sci.*, **32**, 25–59.

Malkus, J. and H. Riehl, 1960: On the dynamics and energy transformations in a steady-state hurricane. *Tellus*, **12**, 1–20.

May, P. T., C. Jakob, J. H. Mather, and G. Vaughan, 2008: Field research: Characterizing oceanic convective cloud systems. *Bull. Amer. Meteor. Soc.*, **89**, 153–155.

McBride, J. L. and T. D. Keenan, 1982: Climatology of tropical cyclone genesis in the Australian region. *J. Clim.*, **2**, 13–33.

Montgomery, M. T., C. Davis, T. Dunkerton, Z. Wang, C. Velden, R. Torn, S. Majumdar, F. Zhang, R. K. Smith, L. Bosart, M. M. Bell, J. S. Haase, A. Heymsfield, J. Jensen, T. Campos, and M. A. Boothe, 2012: The Pre-Depression investigation of cloud systems in the tropics (predict) experiment: Scientific basis, new analysis tools, and some first results. *Bull. Amer. Meteor. Soc.*, **93**, 153–172.

Montgomery, M. T., S. V. Nguyen, R. K. Smith, and J. Persing, 2009: Do tropical cyclones intensify by WISHE? *Quart. Journ. Roy. Meteor. Soc.*, **135**, 1697–1714.

Montgomery, M. T., M. E. Nichols, T. A. Cram, and A. B. Saunders, 2006: A vortical hot tower route to tropical cyclogenesis. *J. Atmos. Sci.*, **63**, 355–386.

Montgomery, M. T., J. Persing, and R. K. Smith, 2015: Putting to rest WISHE-ful misconceptions. *J. Adv. Model. Earth Syst.*, **07**, doi:10.1002/.

Montgomery, M. T. and R. K. Smith, 2011: Tropical cyclone formation: Theory and idealized modelling. *In Proceedings of Seventh WMO International Workshop on Tropical Cyclones (IWTC-VII), La RéUnion, Nov. 2010. (WWRP 2011-1) World Meteorological Organization: Geneva, Switzerland*, pp23, [Available online at http://www.wmo.int/pages/prog/arep/wwrp/tmr/otherfileformats/documents/2_1.pdf].

— 2014: Paradigms for tropical cyclone intensification. *Aust. Met. Ocean. Soc. Journl.*, **64**, 37–66, [Available online at http://www.bom.gov.au/amoj/docs/2014/montgomery_hres.pdf].

Montgomery, M. T., J. A. Zhang, and R. K. Smith, 2014: An analysis of the observed low-level structure of rapidly intensifying and mature Hurricane Earl (2010). *Quart. Journ. Roy. Meteor. Soc.*, **140**, 2132–2146, doi:10.1002/qj.2283.

Nguyen, V. S., R. K. Smith, and M. T. Montgomery, 2008: Tropical-cyclone intensification and predictability in three dimensions. *Quart. Journ. Roy. Meteor. Soc.*, **134**, 563–582.

Ooyama, K. V., 1969: Numerical simulation of the life cycle of tropical cyclones. *J. Atmos. Sci.*, **26**, 3–40.

Persing, J., M. T. Montgomery, J. McWilliams, and R. K. Smith, 2013: Asymmetric and axisymmetric dynamics of tropical cyclones. *Atmos. Chem. Phys.*, **13**, 12299–12341.

Schubert, W. H. and J. J. Hack, 1982: Inertial stability and tropical cyclone development. *J. Atmos. Sci.*, **39**, 1687–1697.

Shapiro, L. J. and M. T. Montgomery, 1993: A three-dimensional balance theory for rapidly-rotating vortices. *J. Atmos. Sci.*, **50**, 3322–3335.

Shin, S.-E. and R. K. Smith, 2008: Tropical-cyclone intensification and predictability in a minimal three dimensional model. *Quart. Journ. Roy. Meteor. Soc.*, **134**, 1661–1671.

Smith, R. K. and M. T. Montgomery, 2010: Observations of the convective environment in developing and non-developing tropical disturbances. *Quart. Journ. Roy. Meteor. Soc.*, **138**, 1721–1739.

— 2015a: The efficiency of diabatic heating and tropical cyclone intensification. *Quart. Journ. Roy. Meteor. Soc.*, **141**, submitted.

— 2015b: Towards clarity on tropical cyclone intensification. *J. Atmos. Sci.*, **72**, 3020–3031.

Smith, R. K., M. T. Montgomery, G. Kilroy, S. Tang, and S. Müller, 2015a: Tropical low formation during the australian monsoon: the events of january 2013. *Aust. Met. Ocean. Soc. Journl.*, **65**, 318–341.

Smith, R. K., M. T. Montgomery, and S. V. Nguyen, 2009: Tropical cyclone spin up revisited. *Quart. Journ. Roy. Meteor. Soc.*, **135**, 1321–1335.

Smith, R. K., J. A. Zhang, and M. T. Montgomery, 2015b: The dynamics of intensification in an HWRF simulation of Hurricane Earl (2010). *Quart. Journ. Roy. Meteor. Soc.*, **141**, submitted.

Tory, K. J., N. E. Davidson, and M. T. Montgomery, 2007: Prediction and diagnosis of tropical cyclone formation in an NWP system. Part III: Diagnosis of developing and nondeveloping storms. *J. Atmos. Sci.*, **64**, 3195–3213.

Trenberth, K. E., C. A. Davis, and J. Fasullo, 2007: Water and energy budgets of hurricanes: Case studies of ivan and katrina. *J. Geophys. Res.*, **112**, doi:10.1029/2006JD008303, d23106.

Črnivec, N. and R. K. Smith, 2016: Mean radiosonde soundings for the Australian monsoon/cyclone season. *Int. J. Climatol.*, **36**, in press.

Vigh, J. L. and W. H. Schubert, 2009: Rapid development of the tropical cyclone warm core. *J. Atmos. Sci.*, **66**, 3335–3350.